Dyes and Pigments 94 (2012) 452–458

Contents lists available at SciVerse ScienceDirect

Dyes and Pigments

journal homepage: www.elsevier.com/locate/dyepig

Reflection characteristics of cholesteric liquid crystal microcapsules with different geometries

Kui Lv, Dongzhi Liu, Wei Li, Qixiang Tian, Xueqin Zhou*

School of Chemical Engineering, Tianjin University, Tianjin 300072, PR China

ARTICLE INFO

Article history:
Received 25 October 2011
Received in revised form
5 February 2012
Accepted 7 February 2012
Available online 13 February 2012

Keywords:
Cholesteric liquid crystals
Solvent evaporation
Microcapsules
Geometry
Selective reflection
Modeling

ABSTRACT

The reflection properties of cholesteric liquid crystals (CLCs) encapsulated in poly(methyl methacrylate) (PMMA) by solvent evaporation were investigated both experimentally and theoretically. The geometry of the CLC/PMMA microcapsules significantly influenced their reflection characteristics. Spherical CLC/PMMA microcapsules exhibit a color corresponding to the CLC intrinsic wavelength λ_0 at the center of the microcapsule with the color changing to colorless at the fringes, whereas flattened spherical CLC/PMMA microcapsules only show vivid color at their centers. By recognizing the effect of the interactions between PMMA and CLC, an alignment model was developed and analyzed. The high correlation between the experimental and modeled color data confirms a high degree of ordering of the CLC molecules inside the microcapsules. The calculated results for a single CLC/PMMA microcapsule were in good agreement with the experimental reflection spectra of the CLC/PMMA microcapsule films. These results show how the shapes of CLC/polymer composites determine their optical properties.

1. Introduction

Cholesteric liquid crystals (CLCs), with their unique property of selective light reflection, have attracted a great deal of attention because of their potential optical applications in areas, such as color displays [1–7], temperature indicators [8], environment monitors [9], tunable laser devices [10], optical filters [11] and supplementary tools for medical diagnosis [12]. The use of CLCs in displays is commonly achieved by incorporating CLCs into a polymer matrix to protect them against adverse environmental effects and to provide a flexible matrix [13,14].

The reflection spectra of CLCs are directly related to their helical pitch and to the direction of the incident light [10,11,15–19]. Introduction of CLCs into a polymer matrix significantly influences their optical properties. Dispersing CLCs in a polymer matrix often initially results in the formation of spherical droplets, however numerous experimental studies have shown that non-spherical CLC droplets, such as flattened spheres [13,14,20–25] and ellipses [26,27], are crucial to achieve the outstanding reflection properties needed for CLC displays (CLCDs). So far, no explanation for this phenomenon has been given. Interactions with the polymer matrix further influence the optical properties of CLC systems by causing interface-induced deformations of the CLC supermolecular structure [28]. However, there are no experimental studies on the optical properties of CLC/polymer microcells [29]. Theoretical treatment of the reflection characteristics of CLC/polymer films is also a complicated problem.

A great deal of work has been done to simplify calculations of the optical properties of CLC/polymer composites. Zharkova et al. [30] investigated the optical properties of aqueous dispersions of CLC microcells. The theoretical and experimental spectral curves of polarized light transmission were consistent throughout the whole visible range, which confirmed a high degree of ordering of the CLC molecules in the spherical cells. Agez et al. [31] reported on the color selectivity of CLCs by monitoring interface-induced deformations. The interactions between the CLCs and the other substances were calculated to evaluate changes in the distribution and to explain the changing colors of the CLC films obtained under various quenching conditions. Chevallard et al. [32] noted that the disappearance of the interface translational invariance or of the reflection symmetry along the wall axis might induce new interfacial patterns. Cox et al. [33] modeled the effect of microencapsulation on the electro-optical behavior of CLC/polymer flakes. The field acting on the flakes was significantly altered by various encapsulating materials and boundary conditions. However, all these calculations ignored the effects of geometries on the optical properties of the CLC microcells.

* Corresponding author. Tel.: +86 2227400911; fax: +86 2227892283.
E-mail address: zhouxueqin@tju.eud.cn (X. Zhou).

0143-7208/$ – see front matter © 2012 Elsevier Ltd. All rights reserved.
doi:10.1016/j.dyepig.2012.02.004

CLCs can be confined in a polymer matrix by microencapsulation (emulsification) [34–36] or phase separation methods [37–39]. The solvent evaporation method has been used to prepare spherical microcapsules with high core loadings, and controllable particle sizes and shell thicknesses. When a "hard" material such as poly(methyl methacrylate) (PMMA) or polycarbonate (PC) is employed as the shell, deformation of the CLC microcapsules may occur upon drying for their thin shells, leading to a controllable microcapsule geometry. In this work, the reflection color characteristics of CLC/PMMA microcapsules obtained by the solvent evaporation method are reported. A model for a single CLC/PMMA microcapsule was constructed to explain the observed phenomena. The reflection spectra of spherical and flattened spherical CLC/PMMA microcapsules were estimated using the model.

2. Experimental

2.1. General

Poly(methyl methacrylate) (PMMA, $M_w = 5.0 \times 10^5 - 1.0 \times 10^6$ gmol^{-1}, refractive index 1.49) and poly(vinyl alcohol) (PVA, $M_w = 8.8 \times 10^4$–9.2×10^4 gmol^{-1}, 88% hydrolyzed) were used as received without further treatment. The red cholesteric liquid crystal (R-CLC) and green cholesteric liquid crystal (G-CLC) (Chengzhi Yonghua, China) have mean reflection wavelengths, λ_0, of 640 and 550 nm respectively. Their refractive indexes of the ordinary (n_o) and extraordinary (n_e) light are 1.51 and 1.49 respectively. All other solvents were reagent grade and were used without further purification.

The morphologies of the microcapsules were analyzed with a scanning electron microscope (SEM, S4800, JP-Hitachi Limited) and an optical microscope (OM, Lv-UEPI, JP-Nikon). The color images of the CLC/PMMA microcapsules were obtained by using a stereo microscope (SMZ1500, JP-Nikon). The reflection spectra of CLC/PMMA microcapsule films were recorded with a UV/VIS/NIR spectrophotometer (UV3600, JP-Shimadzu).

2.2. Preparation of CLC/PMMA microcapsules

PMMA (0.20 g) and CLC (1.00 g) were successively dissolved in dichloromethane (10 mL). Then the solution was added dropwise to a 2 wt% PVA aqueous solution (40 mL) at 20 °C while stirring at 1500 rpm. An O/W emulsion formed after stirring at 1500 rpm for 20 min. Thereafter the agitation rate was decreased to 300 rpm and another aliquot of 2 wt% PVA aqueous solution (40 mL) was added to dilute the emulsion. The emulsion was then heated to 35 °C in 20 min. Afterwards, the organic solvent was removed by evaporation at 35 °C for about 10 h under atmospheric pressure. Finally an aqueous dispersion of CLC/PMMA microcapsules was obtained by washing repeatedly with water via precipitation and decantation.

2.3. Fabrication of CLC/PMMA microcapsule films

The CLC/PMMA microcapsule aqueous dispersion (50 wt%) was added to an aqueous PVA solution (1 wt%) in the weight ratio of 1:1. The mixture was coated on a glass plate and dried to form CLC/PMMA microcapsule films.

2.4. Determination of the core loading of CLC/PMMA microcapsules

About 0.5 g of dry microcapsules were cracked by squeezing, and then extracted with ethanol. The residual solid was collected, dried and weighed. The CLC loading in the microcapsules (C_c%) is calculated as follows:

$$C_c\% = (1 - W_p/W_t) \times 100\% \quad (1)$$

where W_p and W_t are the weights of the residual solid and the dry microcapsules, respectively.

3. Results and discussion

3.1. Characterization of the CLC/PMMA microcapsules

The ratio of polymer shells to CLC cores was adjusted to control the core loading, shell thickness and morphology. As shown in Table 1, the core loading is in good agreement with the initial CLC content. For a mononuclear CLC/PMMA microcapsule with a core loading of C_c%, the shell thickness (t) can be calculated using Eq. (2), where R is the microcapsule radius and ρ_c and ρ_m are the densities of the CLC cores and PMMA shells respectively. Hence microcapsules with different shell thickness can be easily obtained by controlling the initial CLC content.

$$t = \left[1 - \left(\frac{C_c\%/\rho_c}{(1 - C_c\%)/\rho_m + C_c\%/\rho_c}\right)^{1/3}\right] R \quad (2)$$

OM images of the R-CLC/PMMA microcapsules dispersed in water were obtained and are shown in Fig. 1. SEM images of the dried and fractured R-CLC/PMMA microcapsules were also obtained and are shown in Fig. 2. All the microcapsules dispersed in water have a spherical core/shell structure, which indicates that initially a spherical CLC droplet is encapsulated in each microcapsule. After drying, the spherical CLC/PMMA microcapsules became flattened if the core loading is ≥95.25% (Fig. 2b), whereas the microcapsules with lower core loadings (≤83.37%) were still spherical (Fig. 2a). This is probably due to the different shell thicknesses (Table 1). The microcapsule with thin shell is not strong enough to keep its spherical shape when it is dried, which results in the shape deformation of the CLC droplet in the microcapsule (Fig. 2d). On the contrast, the microcapsule with thick shell is still spherical after drying, so its core keeps spherical too (Fig. 2c). If the shell thickness is reduced even further, the microcapsules crack even more easily during drying.

3.2. Reflection colors of the CLC/PMMA microcapsules

Reflection color images of the CLC/PMMA microcapsules were obtained with a stereo microscope and are shown in Fig. 3. The microcapsule diameters were between 5 and 30 μm. As shown in Fig. 3a, the spherical R-CLC/PMMA microcapsules in water are red at the center, change to yellow or green moving away from the center and are colorless at the fringes (for interpretation of the references to colour in this figure, the reader is referred to the web version of this article). The spherical G-CLC/PMMA microcapsules have a central green-blue spot with achromatic rings at the edges (Fig. 3b). The dried R1-CLC/PMMA microcapsules are typically

Table 1
Properties of microcapsules prepared with different R-CLC/PMMA ratios.

Samples	Initial addition		CLC content[a] (wt%)	C_c% [b] (wt%)	Average R (μm)	Average t[c] (nm)
	PMMA(g)	R-CLC(g)				
R1-CLC/PMMA	0.20	1.00	83.33	83.37	14.7	372
R2-CLC/PMMA	0.10	1.00	90.91	90.67	13.2	176
R3-CLC/PMMA	0.05	1.00	95.24	95.25	12.9	88
R4-CLC/PMMA	0.03	1.00	97.09	97.10	10.6	44

[a] Initial CLC content, which is the ratio of the weight of the initial addition of R-CLC to the total addition of R-CLC and PMMA.
[b] R-CLC loading in microcapsules calculated from Eq. (1).
[c] Average shell thickness calculated from Eq. (2).

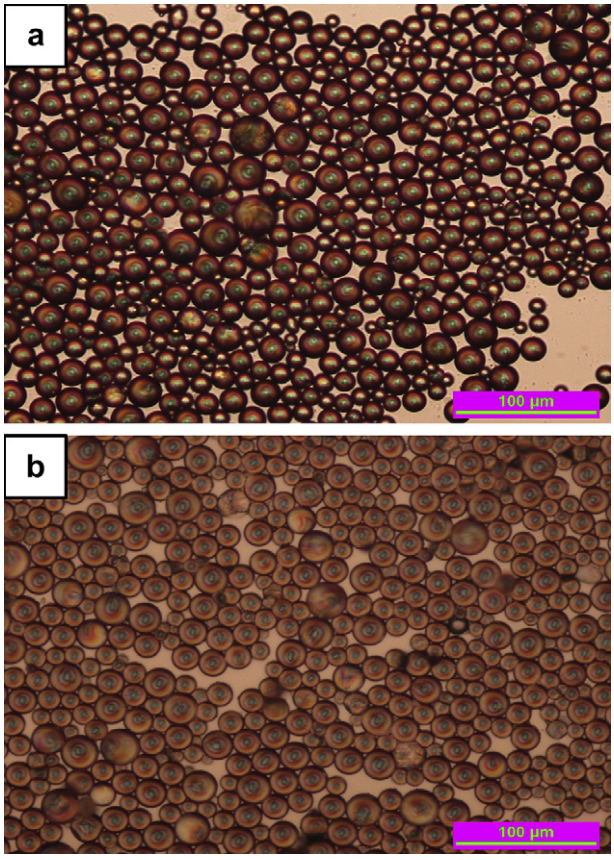

Fig. 1. OM images of the R-CLC/PMMA microcapsules dispersed in water. The core loadings are 83.37wt% (a) and 95.25wt% (b) respectively.

spherical because of their thick shells and have similar colors to the aqueous spheres (Fig. 3c). However, the dried R3-CLC/PMMA microcapsules are flattened spheres because of their thin shells and show only a red center (Fig. 3d).

Furthermore, the dried films prepared with R1-CLC/PMMA microcapsules were white, whereas the dried films of R3-CLC/PMMA microcapsules showed a clear red color. This is obviously due to the different geometries of the dried microcapsules. As observed previously, the dried R3-CLC/PMMA microcapsules are flattened spheres whereas the R1-CLC/PMMA microcapsules maintain their spherical geometry during drying (Fig. 3c and d). These phenomena are consistent with results in the literature showing that non-spherical droplets such as flattened spheres or ellipses are favorable for colorful CLCDs [13,14].

3.3. Calculation of the reflection characteristics of a single CLC/PMMA microcapsule

Mathematical modeling of films made from CLC/PMMA microcapsules is very complex because there are so many factors that can influence the reflection characteristics of the films, including the size and shape of the microcapsules, the interactions between the CLC core and the PMMA shell, the shell thickness, the number of layers of microcapsules, multiple light scattering among the microcapsules and other uncontrollable effects during the processing. A model for a single CLC/PMMA microcapsule was designed and analyzed. To simplify the calculations, the absorption, refraction and scattering of the PMMA shell were all ignored. These influences are minor since the PMMA content in the microcapsules is low.

It was assumed that the CLC aligned in a planar texture with the shell because of the interactions between the CLC and PMMA. Specifically, the rod-like CLC molecules are parallel to the support surface and change regularly in space to form a three-dimensional

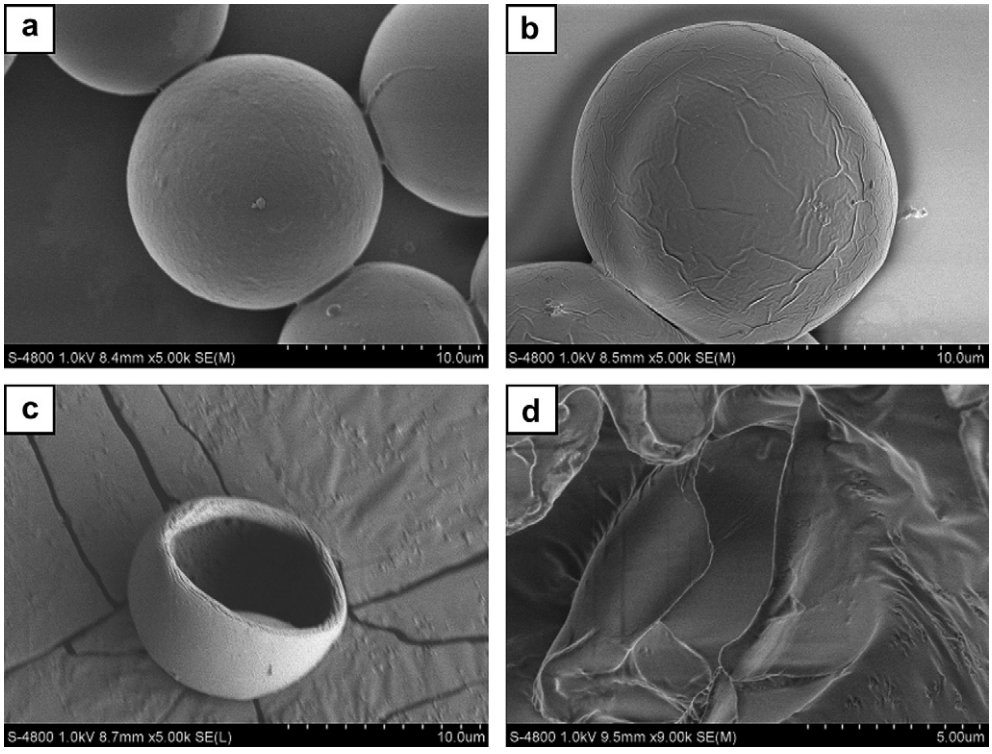

Fig. 2. SEM images of dried R-CLC/PMMA microcapsules and corresponding fractured microcapsules. The core loadings are 83.37wt% (a, c) and 95.25wt% (b, d).

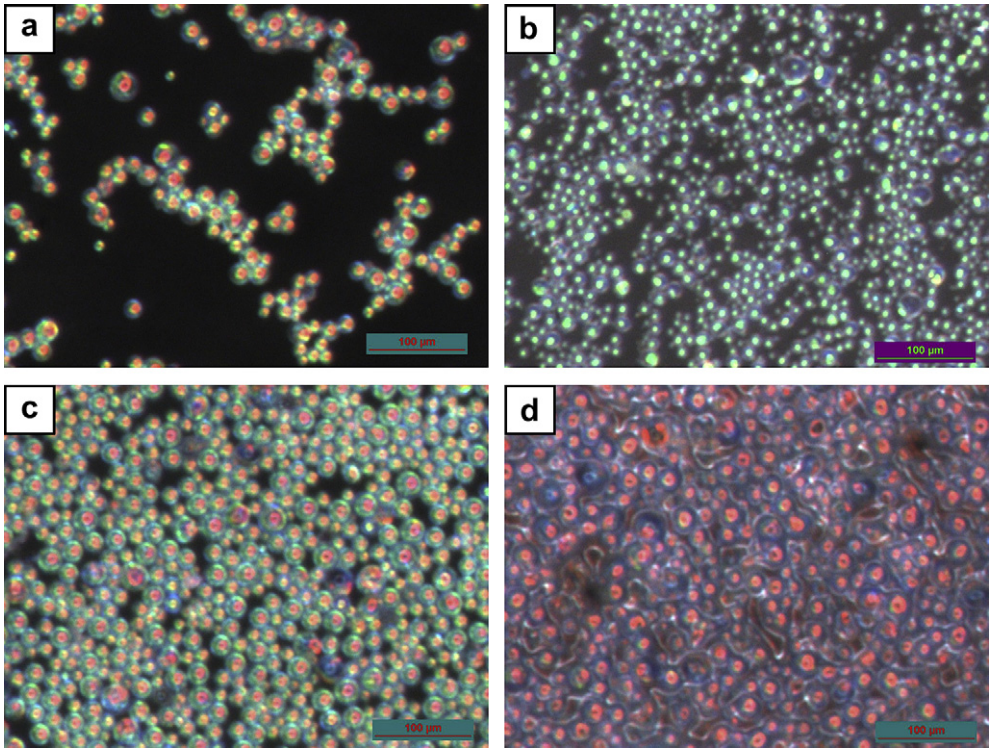

Fig. 3. Stereo microscope images of R-CLC/PMMA microcapsules in water (a), G-CLC/PMMA microcapsules in water (b), dried R1-CLC/PMMA microcapsules (c) and dried R3-CLC/PMMA microcapsules (d).

helix. These interactions have been reported in many experiments [28,31–33,40,41], and similar alignments of CLC have also been proposed to explain related phenomena [31].

3.3.1. Spherical CLC/PMMA microcapsules

The model used to investigate the optical properties of the spherical CLC/PMMA microcapsules is shown in Fig. 4. The planar geometry function is given by

$$X/r = \sin\alpha \tag{3}$$

where X denotes the projective length, r is the radius of the spherical CLC droplet, and α is the angle between the helical axis and the incident light as shown in Fig. 4.

Using the Bragg reflection property, the mean reflection wavelength λ of the CLC at the position with projective length X can be expressed as

$$\lambda(X) = Pn\cdot\cos\alpha \tag{4}$$

where P is the helical pitch, and n is the mean refractive index. Obviously, the mean reflection wavelength at $X = 0(\lambda(0) = Pn)$ also represents the intrinsic mean reflection wavelength λ_0 ($\lambda_0 = Pn$) of the CLC. Thus, the relationship between the mean reflection wavelength $\lambda(X)$ and the projective length X can be expressed as

$$\lambda(X)/\lambda_0 = \cos[\arcsin(X/r)] \tag{5}$$

Plot of this equation is shown in Fig. 5. The ratio of $\lambda(X)$ to λ_0 can vary from 1 to 0 when X increases from 0 to r. That is, for spherical CLC/PMMA microcapsules, the mean reflection wavelength $\lambda(X)$ can vary from 640 to 0 nm when $\lambda_0 = 640$ nm (for R-CLC), or from 550 to 0 nm as $\lambda_0 = 550$ nm (for G-CLC). These results are in good agreement with the experimental changing colors of the spherical CLC/PMMA microcapsules.

For a mononuclear CLC/PMMA microcapsule with a core loading of $C_c\%$ and a radius of R, the radius of the spherical CLC droplet, r, can be calculated by

$$r = \left(\frac{C_c\%/\rho_c}{(1-C_c\%)/\rho_m + C_c\%/\rho_c}\right)^{1/3} R. \tag{6}$$

By combining Eqs. (5) and (6), the ratio of the projective length X to the microcapsule radius R can be expressed as

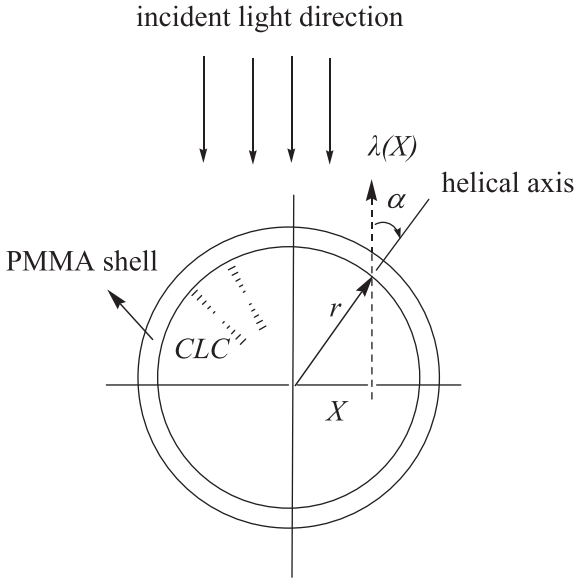

Fig. 4. An ideal spherical CLC/PMMA microcapsule model.

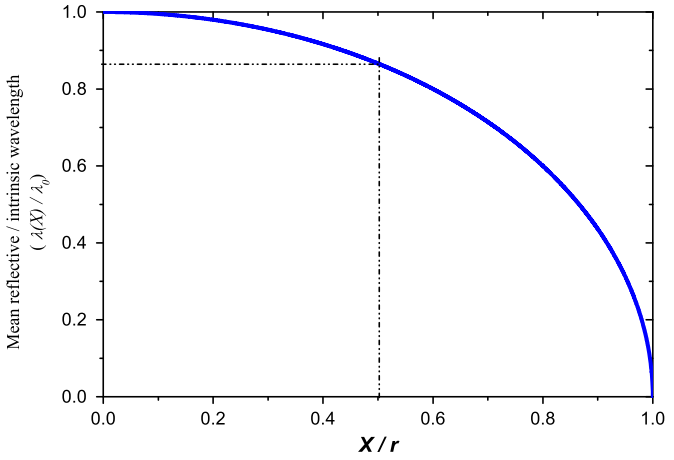

Fig. 5. Plot of the ratio of $\lambda(X)$ to λ_0 versus the ratio of X to r for spherical CLC/PMMA microcapsules.

$$X/R = \left(\frac{C_c\%/\rho_c}{(1-C_c\%)/\rho_m + C_c\%/\rho_c}\right)^{1/3} \times \sin[\arccos(\lambda(X)/\lambda_0)]. \quad (7)$$

Table 2 lists the experimental data from the stereo microscope images of the CLC/PMMA microcapsules together with the corresponding theoretical results from Eq. (7). Considering the errors introduced by the visual resolution, there is good agreement between the calculated data and the experimental results for all four systems.

Mathematically, the ratio of projective area from X_i to X_{i+1} to the whole projective area of the CLC droplet can be expressed as

$$\phi = \frac{\pi x_{i+1}^2 - \pi x_i^2}{\pi r^2} \quad (8)$$

which combined with Eq. (5) and rearranged gives

$$\phi(\Delta\lambda, \lambda, \lambda_0) = \frac{2\Delta\lambda \cdot \lambda}{\lambda_0^2} (\lambda \in [0, \lambda_0]) \quad (9)$$

where $\Delta\lambda = \lambda_i - \lambda_{i+1}$, and $\lambda = (\lambda_{i+1} + \lambda_i)/2$. Here λ_i and λ_{i+1} correspond to the mean reflection wavelengths at positions with projective lengths of X_i and X_{i+1} respectively.

Taking into account the birefringence and the pitch gradient of the CLCs, it can be seen that the practical reflection wavelength of a given CLC is a function of n_e, n_0 and p. Since λ_r is used to represent the detected reflection wavelength of the CLC, it can be expressed as

$$\lambda_r = f(n_e, n_0, p) \quad (10)$$

Table 2
Experimental and calculated results for CLC/PMMA microcapsules.

Samples	C_c% (wt%)	λ_0 (nm)	Color of image fringe	$\lambda(X)$[a]	X/R	
					Mathematical[b]	Experimental[c]
1	83.33	640	Yellow	580	0.4014	0.4036
2	90.91	550	Blue-Green	490	0.4313	0.4425
3	95.24	640	Yellow	580	0.4170	0.4181
4	97.09	550	Blue-Green	490	0.4480	0.4517

[a] Wavelength corresponding to the visual below-limit of the color image fringe. It is employed as the mean reflection wavelength at the corresponding position with a projective length of X.
[b] Calculated according to Eq. (7) with $\rho_c = 1.00\ g\ cm^{-3}$, $\rho_m = 1.19\ g\ cm^{-3}$ (20 °C).
[c] Data is the average value obtained from 200 microcapsules.

Moreover, for a given CLC, there is a corresponding selective reflectivity $\psi(\lambda_r)$, which is approximated by the case of the normal incidence of light on the planar layer of the cholesteric [26]. Therefore, λ_r and $\psi(\lambda_r)$ for different CLCs can be determined by their reflection spectrum. Then, the reflectivity (Γ) for a given incident wavelength (λ) can be expressed as

$$\Gamma(\lambda) = \sum_{i=1}^{i=\infty} [\psi(\lambda_{r,i}) \cdot \phi(\Delta\lambda, \lambda, \lambda_{r,i})] \quad (11)$$

Fig. 6 shows the reflection spectrum of the R-CLC. When $\Delta\lambda$ is set as 1 nm, which is a reasonable value corresponding to the test conditions, the reflection spectrum of a single spherical R-CLC/PMMA microcapsule can be calculated with Eq. (11) by numerical methods. Fig. 7 shows the calculated reflection spectrum of a single spherical R1-CLC/PMMA microcapsule together with the experimental reflection spectrum of the films prepared with spherical R1-CLC/PMMA microcapsules. The simulated result (Fig. 7a) is similar to the experimental reflection spectrum (Fig. 7b). The small discrepancy between curves may be caused by the large number of microcapsules, which leads to multi-scattering among the microcapsules, absorption and scattering of the light by the PVA, and other uncontrollable effect during the processing.

3.3.2. Flattened spherical CLC/PMMA microcapsules

An ideal model of a flattened spherical CLC/PMMA microcapsule with its planar geometry parameters is shown in Fig. 8. The planar geometry parameters for an elliptical CLC droplet with a long axis a and a short axis b can be expressed as

$$\frac{X^2}{a^2} + \frac{Y^2}{b^2} = 1 \quad (12)$$

$$\tan\beta = \frac{L}{Y} \quad (13)$$

$$\frac{Y}{L} = \frac{a^2 Y}{b^2 X} \quad (14)$$

where X, Y and L denote the lengths shown in Fig. 8, β represents the angle between the helical axis and the incident light. Thus, the relationship between the mean reflection wavelength $\lambda(X)$ and the projective length X is given by

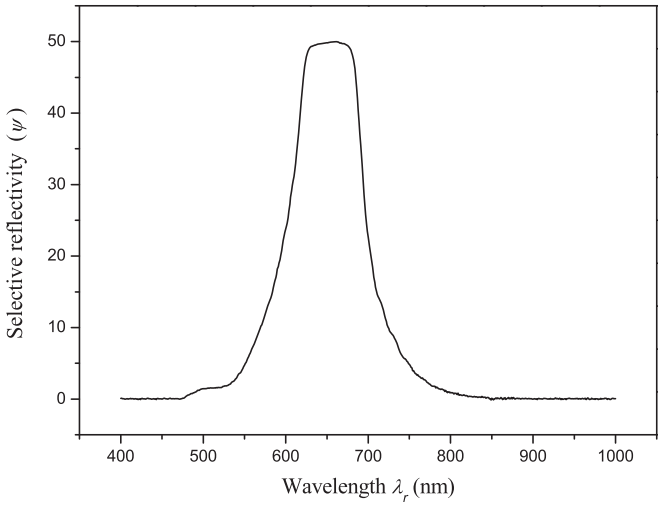

Fig. 6. Reflection spectrum of the planar layer of the R-CLC.

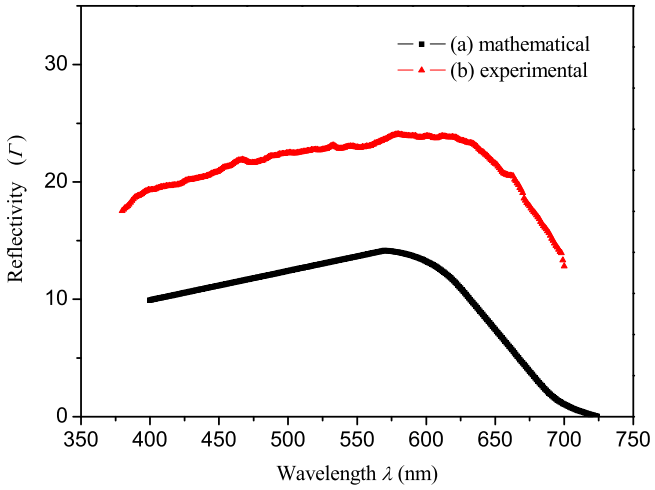

Fig. 7. Calculated reflection spectrum of a single spherical R1-CLC/PMMA microcapsule (a—■—) and experimental reflection spectrum of films prepared with spherical R1-CLC/PMMA microcapsules (b—▲—).

$$\lambda(X)/\lambda_0 = \cos\left(\arctan\frac{bX}{a\sqrt{a^2-X^2}}\right) \tag{15}$$

Plots of Eq. (15) for different ratios of b/a are shown in Fig. 9. The region to reflective wavelength around λ_0 increases as the b/a ratio decreases. Considering the visual resolution, this could explain the phenomena that the dried R3-CLC/PMMA microcapsules only showed a red color at their centers.

Similarly, the ratio of the area of the circle with a projective length from X_i to X_{i+1} to the whole projective area of the CLC droplet can be expressed as

$$\delta = \frac{\pi x_{i+1}^2 - \pi x_i^2}{\pi a^2} \tag{16}$$

which combined with Eq. (15) and rearranged gives

$$\delta(b/a,\Delta\lambda,\lambda,\lambda_0) = \left[\frac{b^2}{a^2}\left(\frac{\lambda_0^2}{(\lambda-\Delta\lambda/2)^2}-1\right)^{-1}+1\right]^{-1} - \left[\frac{b^2}{a^2}\left(\frac{\lambda_0^2}{(\lambda+\Delta\lambda/2)^2}-1\right)^{-1}+1\right]^{-1}, \quad (\lambda\in[0,\lambda_0]) \tag{17}$$

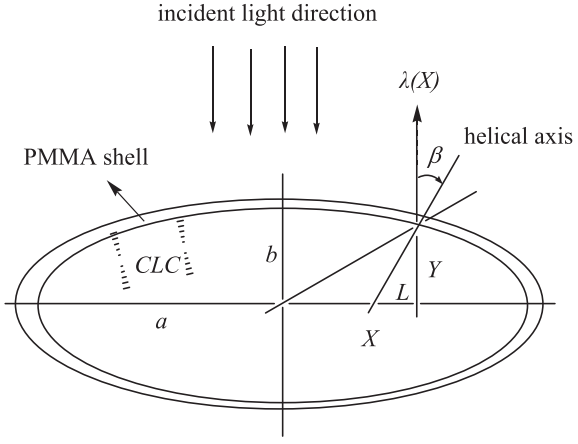

Fig. 8. An ideal flattened spherical CLC/PMMA microcapsule model.

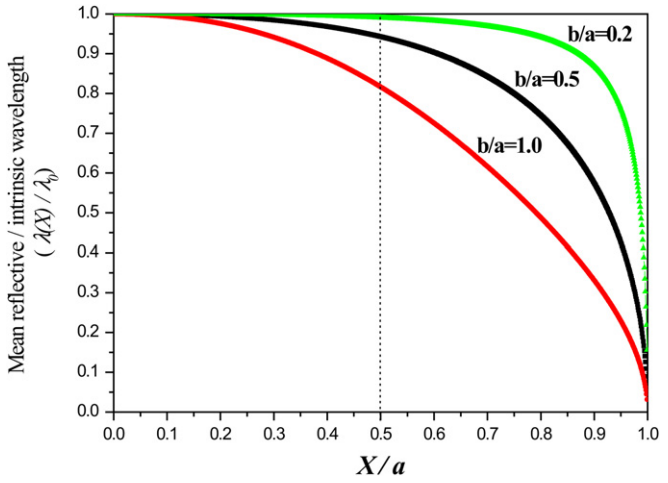

Fig. 9. Plots of the ratio of $\lambda(X)$ to λ_0 versus the ratio of X to a for flattened spherical CLC/PMMA microcapsules.

Taking into account the practical reflection spectrum $\psi(\lambda_r)$ of the CLCs, the reflectivity Γ with a given incident wavelength λ can be expressed as

$$\Gamma(\lambda) = \sum_{i=1}^{i=\infty}\left[\psi(\lambda_{r,i})\cdot\delta(b/a,\Delta\lambda,\lambda,\lambda_{r,i})\right] \tag{18}$$

Eq. (18) can be used to calculate the reflection spectrum of a single flattened spherical R3-CLC/PMMA microcapsule. The calculations used the following physical parameters: $\Delta\lambda = 1$ nm, $b/a = 0.45$ (estimated from the flattened R3-CLC/PMMA microcapsules), $\psi(\lambda_{r,i})$ and $\lambda_{r,i}$ of the R-CLC obtained from Fig. 6. A comparison of the calculated and experimental results is shown in Fig. 10. There is good agreement between the simulated results for a single flattened spherical R3-CLC/PMMA microcapsule (Fig. 10a) and the experimental results from the films constructed from flattened spherical R3-CLC/PMMA microcapsules (Fig. 10b). In fact there is better agreement between the calculated and experimental results for the flattened spherical microcapsules than for the spherical microcapsules. This is probably because there is less PVA filling between the microcapsules in the close-packed flattened spherical microcapsules.

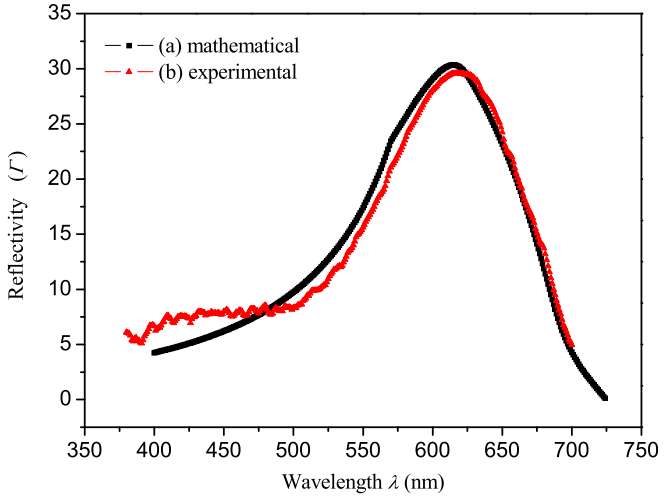

Fig. 10. Calculated reflection spectrum of a single flattened spherical R3-CLC/PMMA microcapsule (a—■—) and experimental reflection spectrum of films prepared with flattened spherical R3-CLC/PMMA microcapsules (b—▲—).

4. Conclusions

The reflection characteristics of CLC/PMMA microcapsules were investigated both experimentally and theoretically. The geometry of the CLC/PMMA microcapsules significantly influences the microcapsule color and reflection spectra. Spherical CLC/PMMA microcapsules can reflect a broadband of wavelengths ($0-\lambda_0$) without distinct selectivity, whereas flattened spherical CLC/PMMA microcapsules only display a narrow band of wavelengths with clear selectivity. An alignment model was used to calculate the optical characteristics of the different microcapsules and to explain the experimental observations. The agreement between the modeled and experimental color data confirms a high degree of ordering of the CLC molecules in the microcapsules. Furthermore, good agreement between the theoretical results for a single CLC microcapsule and the experimental reflection spectra of the CLC/PMMA microcapsule films also supports the alignment model. These results show how the shapes of the CLC microcells determine their optical properties. The data also give a quantitative explanation about why non-spherical CLC microcells, such as flattened spheres and ellipses, are crucial to achieve outstanding reflection properties in CLCDs. The proposed models provide reliable simulations of the optical characteristics of CLC/polymer films constructed with various shapes of CLC microcells.

Acknowledgements

The authors would like to thank Dr. Yumei Hu of Tianjin University for the discussion of the mathematical treatment and the National Nature Sciences Foundation of China (gs1) for the financial support (No. 20976122).

References

[1] Liang HH, Wu CC, Wang PH, Lee JY. Electro-thermal switchable bistable reverse mode polymer stabilized cholesteric texture light shutter. Opt Mater 2011;33:1195–202.
[2] Guo JB, Liu F, Chen FJ, Wei J, Yang H. Realization of cholesteric liquid-crystalline materials reflecting both right- and left-circularly polarized light using the wash-out/refill technique. Liq Cryst 2010;37:171–8.
[3] Tan QF, Zhang Y, Yan YB, Jin GF. High efficiency color separation method based on fractional Talbot effect for color liquid crystal display. Opt Commun 2008; 281:5949–53.
[4] Wu ST, Yang DK. Reflective liquid crystal displays. Chichester, UK: Wiley; 2001.
[5] Li Q, Green L, Venkataraman N, Shiyanonvskaya I, Khan A, Urbas A, et al. Reversible photoswitchable axially chiral dopants with high helical twisting power. J Am Chem Soc 2007;129:12908–9.
[6] Li Q, Li Y, Ma J, Yang DK, White TJ, Bunning TJ. Directing dynamic control of red, green and blue reflection enable by a light –driven self-organized helical superstructure. Adv Mater 2011;23:5069–73.
[7] Ma J, Li Y, White T, Urbas A, Li Q. Light-driven nanoscale chiral molecular switch: reversible dynamic full range color phototuning. Chem Commun 2010;46:3463–5.
[8] Enz E, Lagerwall J. Electrospun microfibres with temperature sensitive iridescence from encapsulated cholesteric liquid crystal. J Mater Chem 2010; 20:6866–72.
[9] Sutarlie L, Qin H, Yang KL. Polymer stabilized cholesteric liquid crystal arrays for detecting vaporous amines. Analyst 2010;135:1691–6.
[10] Manabe T, Sonoyama K, Takanishi Y, Ishikawa K, Takezoe H. Toward practical application of cholesteric liquid crystals to tunale lasers. J Mater Chem 2008; 18:3040–3.
[11] Huck NPM, Staupe I, Thirouard A, Deboer DKG. Light polarization by cholesteric layers. Jpn J Appl Phys 2003;42:5189–94.
[12] Woltman SJ, Jay GD, Crawford GP. Liquid crystals. Singapore: World Scientific; 2007.
[13] Shiyanovskaya I, Green S, Khan A, Magyar G, Pishnyak O, Doane JW. Substrate-free cholesteric liquid-crystal displays. JSID 2008;16:113–5.
[14] Schneider T, Davis DJ, Franklin S, Venkataraman N, Daniel DM, Nicholson F, et al. New development in flexible cholesteric liquid crystal displays. Proc SPIE 2007;6487:64870J–5J.
[15] Zografopoulos DC, Kriezis EE, Mitov M, Binet C. Theoretical and experimental optical studies of cholesteric liquid crystal films with thermally pitch gradients. Phys Rev E 2006;73:061701–9.
[16] Chen T, Feng SM, Xie JN. The new matrix and the polarization state of the transmitted light through the cholesteric liquid crystal. Optik 2010;121: 253–8.
[17] Song K, Park HS, Kim SS, Kim I. Variations of pitch gradient in cholesteric liquid crystal films. PP '2004 Dail international symposium on polymer physics preprints, China; 2004.
[18] Boudet A, Binet C, Mitov M, Bourgerette C, Boucher E. Microstructure of variable pitch cholesteric films and its relationship with the optical properties. Eur Phys J E 2000;2:247–53.
[19] Eelkema R, Pollard MM, Katsonis N, Vicario J, Broer DJ, Feringa BL. Rotational reorganization of doped cholesteric liquid crystalline films. J Am Chem Soc 2006;128:14397–407.
[20] Huiji N, Yamamoto S. Liquid crystal microcapsule, method for producing the same, and liquid crystal display device using the same, US Patent 7,662,444; 2010.
[21] Shiyanovskaya I, Barua S, Green S, Khan A, Greg M, Marhefka D, et al. Single substrate coatable multicolor cholesteric liquid crystal displays. SID Intl Symp Digest Tech Papers 2007;38:65–8.
[22] Khan A, Shiyanovskaya I, Montbach E, Schneider T, Nicholson F, Miller N, et al. Recent advances in flexible low power cholesteric LCDs. Proc SPIE 2006;0225: 0225131–7.
[23] Khan A, Schneider T, Miller N, Ernst T, Nicholson F, Doane JW. Recent advances and product enhancements in reflective cholesteric displays. Proc SPIE 2005;5741:1–6.
[24] Shiyanovskaya I, Khan A, Green S, Magyar G, Pishnyak O, Doane JW. Rugged and drapable cholesteric liquid crystal displays. Proc SPIE 2005;5801:204–12.
[25] Khan A, Shiyanovskaya I, Schneider T, Miller N, Ernst T, Marhefka D, et al. Reflective cholesteric displays: from rigid to flexile. JSID 2005;13:469–74.
[26] Filpo GD, Nicoletta FP, Chidichimo G. Cholesteric Emulsions for colored displays. Adv Mater 2005;17:1150–2.
[27] Kosc TZ, Marshall KL, Petkoska AT, Kimball E, Jacobs SD. Progress in the development of polymer cholesteric liquid crystal flakes for display applications. Displays 2004;25:171–6.
[28] Zharkova GM, Samsonova IV, Streltsov SA, Khachaturyan VM. Structural effect on optical properties in liquid crystal composites. J Struct Chem 2001;42: 315–8.
[29] Leon TL, Nieves AF. Drops and shells of liquid crystal. Colloid Polym Sci 2011; 289:345–9.
[30] Zharkova GM, Streltsov SA, Khachaturyan VM. Aqueous dispersions of cholesteric liquid crystals and their optical properties. J Struct Chem 1999;40: 419–23.
[31] Agez G, Bitar R, Mitov M. Color selectivity lent to a cholesteric liquid crystal by monitoring interface-induced deformations. Soft Mater 2011;7:2841–7.
[32] Chevallard C, Clerc M, Coullet P, Gilli JM. Interface dynamics in liquid crystals. Eur Phys J E 2000;1:179–88.
[33] Cox GP, Marshall KL, Lambropoulos JC, Leitch M, Fromen C, Jacobs SD. Modeling the effects of microencapsulation on the electro-optic behavior of polymer cholesteric liquid crystal flakes. J Appl Phys 2009;106:1249101–12.
[34] Schneider T, Nicholson F, Chien LC. Polymerization-encapsulated cholesteric liquid crystal for bistable reflective displays, US Patent 7,351,506; 2008.
[35] Kim JW, Lee KS, Ju HK, Ryu JH, Han SH, Chang IS, et al. Microencapsulation of cholesteryl alkanoate by polymerization-induced phase separation and its association with drugs. J Polym Sci A 2004;42:2202–13.
[36] Hodson TL, Cartmell JV, Kettering DC, Jones JW. Encapsulated cholesteric liquid crystal display devices, US Patent 3,585,381; 1971.
[37] Ma J, Shi L, Yang DK. Bistable polymer stabilized cholesteric texture light shutter. Appl Phys Express; 2010. doi:10.1143/apex3021702.
[38] Kang SW, Sprunt S, Chien LC. Polymer-stabilized cholesteric diffraction gratings: effect of UV wavelength on polymer morphology and electro-optic properties. Chem Mater 2006;18:4436–41.
[39] Mucha M. Polymer as an important component of blends and composites with liquid crystal. Prog Polym Sci 2003;28:837–73.
[40] Dierking I. Recent developments in polymer stabilised liquid crystals. Polym Chem 2010;1:1153–9.
[41] Suna KR, Woo JY, Cho YH. Interface modification of polymer stabilized cholesteric liquid crystal. Polym Advan Technol 2009;20:501–6.